Peak Forces in High-Resolution Imaging of Soft Matter in Liquid

Horacio V. Guzman, Alma P. Perrino, and Ricardo Garcia*

Instituto de Ciencia de Materiales de Madrid, CSIC 28049 Madrid, Spain

ABSTRACT

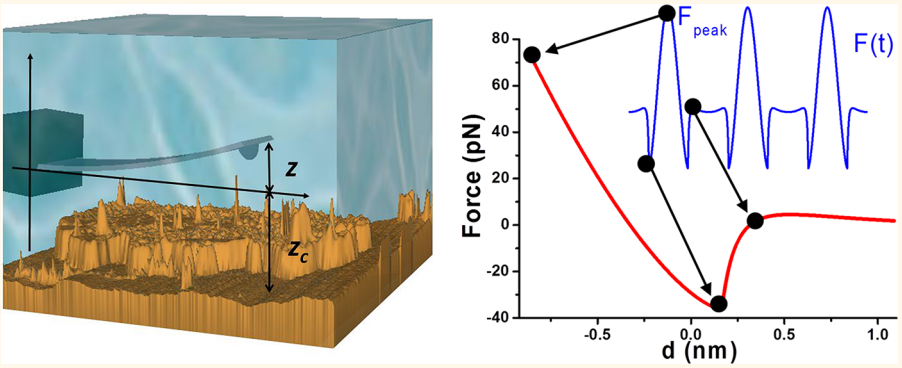

The maximum force exerted by the tip of a force microscope on the sample surface is a critical factor that determines the spatial resolution and the degree of invasiveness of the measurement, in particular, on soft materials. Here we determine the conditions needed to image soft matter in the 30—500 MPa range while applying very small forces. Imaging at sub-50 pN in the elastic regime can only be achieved under strict conditions in terms of force constant values (below 0.1 N/m) and free amplitudes (below 2 nm). The peak force depends on the operational parameters, probe properties, the elastic and/or viscoelastic response of the sample, and the contact mechanics model. Images of heterogeneous samples are never taken at a constant peak force. Under the same operational conditions, smaller forces are obtained on the more compliant materials. We also find that the viscoelastic response reduces the peak force with respect to the purely elastic regions. Our findings are summarized in three-dimensional maps that contain the operational conditions for imaging at low forces.

KEYWORDS: force microscopy · peak forces · soft matter · nanomechanics · deformation

Dynamic atomic force microscopy (AFM) is the most common method to generate atomic and molecular resolution images of soft matter in liquid.[1−13] It has been developed or applied to image with high-resolution polymer surfaces, isolated proteins, or packed arrays of proteins. Dynamic AFM in liquid offers a variety of experimental configurations[10−18] that go from acoustic to magnetic excitation[14−16] or from amplitude[1−3] to frequency modulation AFM methods.[4,5,11,17,18] The use of sharp probes is generally acknowledged as a necessary condition to achieve high-resolution images.[19−21] Another critical factor is the applied force.[22] Force is the physical quantity sensed by the AFM probe; however, the value of the applied force determines the spatial resolution and the degree of invasiveness or nondestructive character of the measurement.[22−24] A key test to determine the degree of invasiveness of a force microscopy measurement can be deduced by comparing the apparent AFM height of a protein and its nominal height. For IgM antibodies in water,[11] this requires the application of forces below 50 pN. Similarly, the applied force determines the type of information retrieved while imaging biological membranes in liquid.[24] Muller *et al.* found that, in order to properly measure bacteriorhodopsin, loop forces below 100 pN were required.[24] Sub-50 pN forces are claimed but not measured in molecular resolution and high-speed AFM images of proteins.[2,25] Thus, it can be concluded that high-resolution and noninvasive imaging can only be achieved by the application of very small forces.

Forces are directly sensed by the AFM probe; however, they are not directly measured

* Address correspondence to r.garcia@csic.es.

Received for review December 14, 2012 and accepted March 16, 2013.

Published online March 22, 2013
10.1021/nn4012835

in dynamic AFM. The nonlinear character of the tip–sample force prevents the deduction of analytical expressions to calculate the maximum force (peak force). Several force inversion methods have been proposed;[26−30] however, their application has not been generalized because their accuracy has not been fully verified. In addition, those methods require the simultaneous and accurate recording of the amplitude and phase shift curves. As a consequence, most AFM experiments do not provide information about the forces used to generate the images. This complicates the comparison among images obtained by different dynamic AFM approaches which, in turns, limits the reproducibility and slows down the progress toward obtaining routinely molecular resolution images. Different models and numerical simulations offer insight into the dynamics of the probe motion.[9,16,31−37] Raman *et al.* have proposed a parametrized expression to calculate the peak force in air.[33] That expression has been applied to study relatively stiff viral capsids (>1 GPa) in liquid.[34] However, detailed calculations of the peak forces applied while imaging soft matter at high resolution in liquid (sub-1 nN forces) have not been provided.

Here we have performed an extensive study of the forces applied in amplitude modulation atomic force microscopy while imaging soft matter in liquid. We have used two contact mechanics models, the widely used Hertz model[38] and the rarely used Tatara model.[39−41] The calculations have been performed to simulate a wide range of materials and experimental parameters. The sample elastic modulus E_s (Young's modulus) and viscosity coefficient η_s range, respectively, from 30 to 500 MPa and 0 to 100 Pa·s.

The results show a nonlinear dependence of the peak force on the local elastic modulus of the sample and the set-point amplitude A_{sp}. Under the same operational conditions, that is, tip radius R_t, force constant k, free A_0, and set-point A_{sp} amplitudes, the peak force increases with the elastic modulus. This result is at odds with some simple approximations deduced by extension of Hooke's law.[42] However, it is in agreement with the parametrized expression deduced by Hu and Raman.[33] In addition, we show that on soft matter the peak force has a non-negligible contribution from the cantilever deflection. Tatara and Hertz models give the same qualitative trend. However, under the same conditions, higher peak forces are given by Hertz contact mechanics. We consider that Tatara's model could provide a better description of the deformation and forces involved in AFM experiments of biomolecules than the Hertz's model because it explicitly addresses their finite size.

Figure 1 shows a scheme of the experimental setup and the deformation induced on a soft material by the tip's load according to Hertz and Tatara models. The deformation and consequently the maximum force induced by the tip depends on both the operational parameters such as the free and set-point amplitudes, the probe parameters such as the force constant, the radius and the sample elastic modulus, and the contact mechanics model used to describe the experiment.

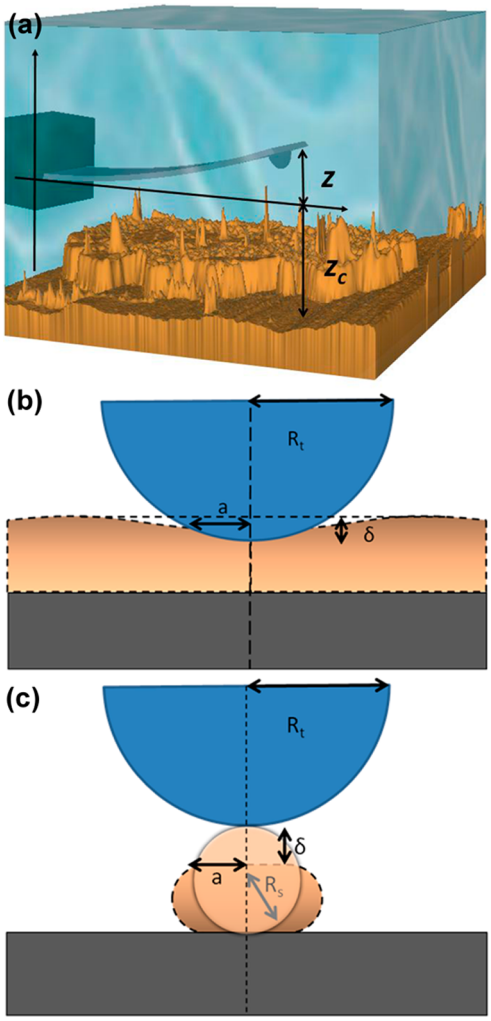

Figure 1. (a) Scheme of the probe–surface interface in liquid. (b) Scheme of the sample deformation in the Hertz model and definition of the tip's radius, contact area, and indentation. (c) Scheme of the sample deformation in the Tatara model and definition of the tip's and sample radii, contact area, and indentation.

RESULTS AND DISCUSSION

A detailed description of the equation of motion, the numerical simulations, and the modelization of the tip–surface forces is found in Methods. Here, the tip–surface force includes contributions from repulsive contact mechanics forces (as given by Hertz or Tatara), Derjaguin–Landau–Verwey–Overbeek (DLVO) electrostatic forces,[43] and viscoelastic forces deduced from linear approximations, then

$$F_{ts} = F_{Hertz(Tatara)} + F_{DLVO} + F_v \quad (1)$$

Figure 2 illustrates the definition of the peak force in time-varying force plots. The curves show a repulsive

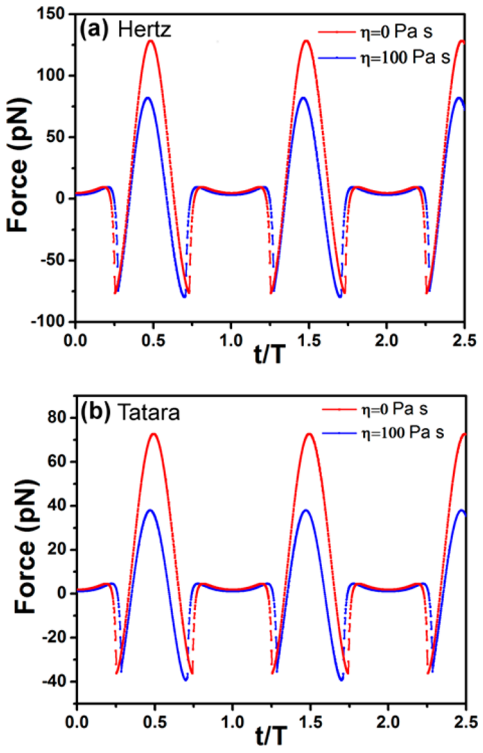

Figure 2. Time-varying force for E_s = 50 MPa with and without viscous response. The simulations include DLVO forces. For each curve, the maximum value in the force curve is the peak force. Two full oscillations are shown: (a) Hertz; (b) Tatara.

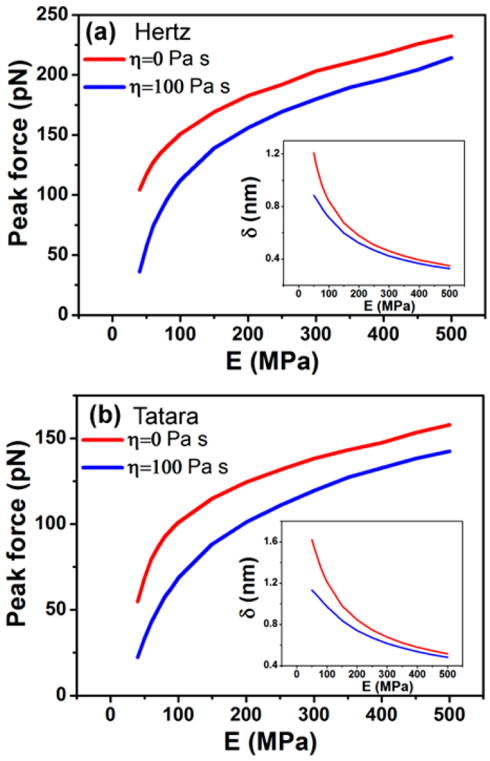

Figure 3. (a) Dependence of the peak force as a function of the sample's Young's modulus for elastic (Hertz) and viscoelastic responses. (b) Dependence of the peak force as a function of the sample's Young's modulus by using Tatara. Simulation data, k = 0.2 N/m, f_0 = 25 kHz, Q = 2, A_0 = 1 nm, $A_{sp} = 0.9A_0$, R_t = 5 nm, and R_s = 4 nm.

tail followed by a short attractive region (both coming from DLVO forces) which ends once the tips establishes mechanical contact with the surface. There are two additional observations. First, under the same operational conditions, Hertz contact mechanics gives larger forces than Tatara. Second, the peak force is reduced by considering a viscoelastic response.

The behavior of the peak force as a function of the sample's Young's modulus in the range of 30 to 500 MPa is plotted in Figure 3. This figure shows that the force given by Hertz increases with E_s from 100 pN (E_s = 40 MPa) to 230 pN at 500 MPa (elastic case). The peak force is reduced significantly by using Tatara. For the same range of E_s, the force goes from 55 to 155 pN. This trend is preserved when the material has a viscoelastic response, although the values of the peak forces are smaller. Increasing E_s reduces the role of the viscous force because the indentation is smaller (see insets) than the contribution from viscoelasticity (see eq 12).

The dependence of the peak force with the material might be surprising because the simulations have been performed for the same operational parameters (A_0 = 1 nm, A_{sp} = 0.9 nm) and the tip's values (k = 0.2 N/m, R_t = 5 nm, Q = 2, and f_0 = 25 kHz). The above dependence shows that the transformation of the kinetic energy from the tip into the sample's potential energy is mediated by other factors such as the contact time and the deformation. Under the same operational conditions, the stiffer the material, the higher the peak force, and the shorter the contact time. This result implies that imaging of heterogeneous surfaces is never accomplished at a constant peak force value.

Tatara contact mechanics releases the vertical load into both vertical and lateral deformations, which, in turn, reduces the peak force with respect to Hertz. It also considers the object with a finite size. However, the qualitative behavior of the curves is independent of the contact mechanics model. For the above reasons, the Tatara model (with the addition of DLVO and viscoelastic forces) has been used to generate the data shown in Figures 4–6.

Figure 4 shows the dependence of the peak force with A_{sp}. For E_s = 50 MPa, the peak force shows a small increase with decreasing A_{sp} from A_0 to $0.75A_0$. For lower A_{sp} values, the graph shows a sudden increase. This behavior is not present in stiffer materials (E_s = 500 MPa). For viscoelastic materials, the sudden increase of the peak force is still present for E_s = 50 MPa (Figure 4b). For stiff materials, the curves show a maximum with A_{sp}.

The above results underline the different response between soft and stiff materials to the tip interactions. They also show the existence of two different mechanisms for the generation of peak force values. In the absence of dissipation, the reduction of the amplitude

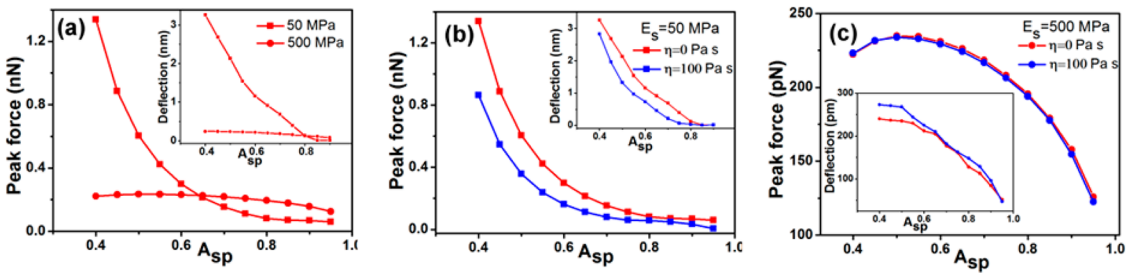

Figure 4. Dependence of the peak force with the set-point amplitude. (a) $E = 50$ MPa, $\eta = 0$, and 100 Pa s. (b) $E = 50$ MPa, $\eta = 0$, and 100 Pa s. The insets show the dependence of the deflection with respect to A_{sp}. Contact mechanics by Tatara. Simulation data, $k = 0.2$ N/m, $f_0 = 25$ kHz, $Q = 2$, $A_0 = 1$ nm, $A_{sp} = 0.9A_0$, $R_t = 5$ nm, and $R_s = 4$ nm.

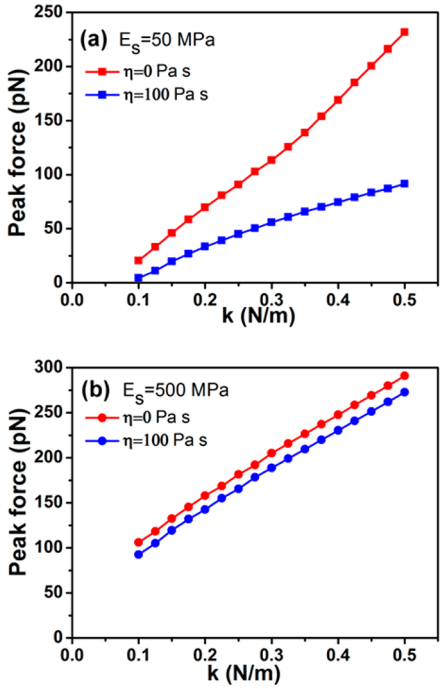

Figure 5. Dependence of the peak force with the force constant. Contact mechanics by Tatara. Simulation data, $k = 0.2$ N/m, $f_0 = 25$ kHz, $Q = 2$, $A_0 = 1$ nm, $A_{sp} = 0.9A_0$, $R_t = 5$ nm, and $R_s = 4$ nm.

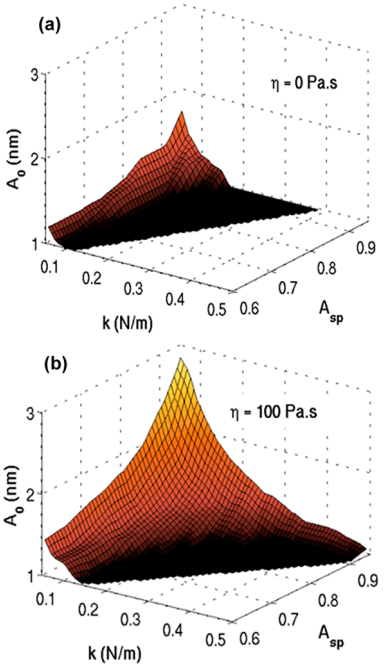

Figure 6. Three-dimensional maps of the dynamic AFM operational parameters that establish a given peak force (here 75 pN) for a material with a Young's modulus of $E = 50$ MPa: (a) elastic; (b) $\eta = 100$ Pa·s. Simulation data, $f_0 = 25$ kHz, $Q = 2$, $R_t = 5$ nm, and $R_s = 4$ nm. Contact mechanics by Tatara.

is caused by the detuning of the resonance curve.[44] For high Young's modulus materials, the peak force follows the trend of the minimum tip−surface distance with A_{sp}, which has a minimum.[45] However, for soft materials and small A_{sp} values, the amplitude can only be reduced by introducing a significant tip deflection. A positive tip deflection is achieved by the feedback mechanism that moves the z position of the sample with respect to the tip until the A_{sp} is reached. This interpretation is confirmed by observing the correlation between the peak forces and the cantilever deflection (insets in Figure 4). In soft matter, the presence of high values of the cantilever deflection (relative the oscillation amplitude) implies that the tip is in contact with the sample during the whole oscillation cycle.

The dependence of the peak force with the cantilever force constant is shown in Figure 5 for two different values, 50 and 500 MPa ($A_{sp} = 0.9A_0$, $A_0 = 1$ nm). In both cases, the dependence of F_{peak} with k is almost linear, although some minor deviations are observed for low force constants. In this case, the peak force follows the trend of Hooke's law.

Three-dimensional plots of the dependence of the peak force with both the force constant and the free amplitude provide a summary of the operational conditions required to acquire images at a given peak force (Figure 6). They could also provide guidelines to achieve low forces in an experiment. The plots illustrate the requirement of using small amplitudes to reduce the force. Specifically, a peak force of 75 pN requires the use of a free amplitude below 2 nm. It is interesting to note that the introduction of viscoelasticity slightly enlarges the operational space in all of the axes. For example, the free amplitude goes from 1.8 nm (elastic) to 2.9 nm ($\eta = 100$ Pa·s) ($A_{sp} = 0.95A_0$). However, the peak force reduction due to a viscoelastic response

TABLE 1. Peak Force as a Function of E_s and A_0 (k = 0.1 N/m, f_0 = 25 kHz, $A_{sp} = 0.9A_0$, R = 5 nm)

	F_{peak} (pN)			
	A_0 = 1 nm		A_0 = 2 nm	
E_s (MPa)	Q = 1	Q = 2	Q = 1	Q = 2
50	24	7	87	43
75	42	18	119	67
100	55	27	141	85
200	89	59	197	127
300	108	75	231	150
400	122	85	256	168
500	132	92	278	184

maybe misleading because the viscous force could also introduce some irreversible deformations.

In the presence of a viscoelastic response, the average energy supplied by the eternal excitation to the cantilever W_{ext} must be equal to the energy dissipated in the water by hydrodynamic forces W_{med} and in the sample[46] E_{dis}

$$W_{ext} = W_{med} + E_{dis} \quad (2)$$

mechanical energy transferred from the tip to the sample is divided between the elastic deformation (peak force) and the dissipation associated with the viscous force. For example, for $k = 0.1$ N/m, $A_0 = 2.5$ nm, $A_{sp} = 0.9A_0$, and $\eta = 100$ Pa·s, we obtain $W_{med} = 4.96$ eV and $W_{ext} = 5.49$ eV while the energy dissipated in the sample is 0.51 eV. The value of E_{dis} is smaller than the maximum potential energy stored in the tip ($E_p = 0.5kA_{sp}^2 = 1.58$ eV); however, it could imply some damage in molecular resolution measurements.

High-resolution imaging of biomolecular processes at high speed represents one of the more recent and exciting developments of force microscopy.[2,25,42] Ideally, those measurements should be performed at very low forces to minimize sample damage and to avoid external perturbations. In those experiments, the forces were estimated by using an expression derived from Hooke's law

$$F_{peak} = \frac{k(A_0 - A_{sp})}{Q} \quad (3)$$

The above expression is not appropriate for two reasons. First, it does not include any dependence on the material properties. Second, it underestimates the values of the peak forces by at least a factor of 3. For example, it gives a value of 20 pN (k = 0.1 N/m, A_0 = 2 nm, $A_{sp} = 0.9A_0$, Q = 1), while the simulations give 87 and 141 pN, respectively, for E_s = 50 and 100 MPa. The Young's modulus of small to medium size proteins falls in the 10−100 MPa range. Table 1 summarizes the peak forces for some selected Young's modulus and operational parameters.

CONCLUSION

We have calculated the peak force during the AFM imaging of soft matter in liquid as a function of both sample properties and instrumental parameters. Specifically, we have focused our study on soft materials with Young's modulus ranging between 30 and 500 MPa. The mechanical response of the sample has been simulated by using both the standard Hertz contact mechanics and the Tatara model which considers the finite size of the sample. We have calculated three-dimensional maps that show the interplay between different operational parameters to image soft matter at small peak forces. Those forces are the ones required to image noninvasively most proteins. The results show marked qualitative and quantitative differences between soft and stiff materials. We summarize main findings:

(a) Under the same operational and probe conditions, the peak force depends on the elastic properties of the material. The stiffer the material, the larger the peak force. As a consequence, images of heterogeneous samples cannot be taken at a constant peak force.

(b) A viscoelastic response enables the reduction of the peak force.

(c) The amplitude reduction in stiff materials is dominated by the detuning effect. In soft matter, in addition to the above factor, the presence of a positive cantilever deflection is a factor that contributes to the amplitude reduction and then to the peak force.

(d) Imaging soft matter (E_s = 50 MPa) at peak forces below 75 pN requires the use of free amplitudes below 2 nm (elastic regime).

(e) The contact mechanics model has a significant influence on the measured force. For soft materials, the Tatara model gives peak forces that are a factor of 2 smaller than the forces given by the Hertz contact mechanics.

METHODS

To describe the dynamics of the cantilever−tip system and calculate the forces, we model the cantilever as a point-mass model:[43]

$$m\ddot{z}(t) = -kz(t) - \frac{m\omega_0}{Q}\dot{z}(t) + F_{ts}(d) + F_0\cos\omega t \quad (4)$$

where m is the effective cantilever mass that includes the added mass of the fluid, ω_0 is the angular resonant frequency, Q the quality factor, and F_{ts} represents the tip−sample forces. The numerical solution of eq 4 is calculated by using a fourth-order Runge−Kutta algorithm.[43] The use of eq 4 in low Q environments is valid for directly excited cantilevers (magnetic or photothermal excitation). The values used for the resonant frequency, quality factor, and the tip's radius are, respectively, f_0 = 25 kHz, Q = 2, and R_t = 5 nm. The deformation of the sample and thus the contact mechanics forces are described by either Hertz[38] or Tatara

models.[39−41] The repulsive force given the by Hertz is calculated by

$$F_{\text{Hertz}} = \frac{4}{3}E_{\text{eff}}\sqrt{R_t}\delta^{3/2} \quad (5)$$

Tatara model aims to overcome some limitations of the Hertz model; namely, the contact region is not required to be flat, and the finite size of the sample is taken into account. Thus deformation happens in both the tip−sample and sample−solid support contact surfaces. In Tatara's, the repulsive force is given by

$$F_{\text{Tat}} = \frac{\alpha}{2^{3/2}}\delta^{3/2} + \left(\frac{3\alpha^2}{8n_c}\right)\delta^2 + \left(\frac{15\alpha^3}{2^{11/2}n_c^2}\right)\delta^{5/2} \quad (6)$$

where

$$\alpha = \frac{4}{3}\sqrt{R_{\text{eff}}}E_{\text{eff}} \quad (7)$$

$$\frac{1}{E_{\text{eff}}} = \frac{1-\nu_t^2}{E_t} + \frac{1-\nu_s^2}{E_s} \quad (8)$$

$$\frac{1}{R_{\text{eff}}} = \frac{1}{R_t} + \frac{1}{R_s} \quad (9)$$

$$n_c = \frac{4\pi E_t R_t E_s R_s}{6 + \nu_t - 2\nu_t^2 + \nu_s - 2\nu_s^2} \quad (10)$$

In the above equations, δ is the indentation, ν is the Poisson coefficient ($\nu_t = 0.3$ and $\nu_s = 0.45$) where the subindices t and s indicate, respectively, tip and sample), and $E_t = 170$ GPa. The sample indentation is treated differently in Hertz and Tatara. In the Tatara model, the sample is deformed symmetrically on both sides, the probe sample and the sample substrate. In eq 6, the indentation is the addition of both deformations. In Hertz, the deformation only happens in the region where the probe is in contact with the sample. Consequently, for the same peak force, the indentation is higher in Tatara (see insets in Figure 3).

We only consider a viscoelastic response in the linear regime. The viscous force for Tatara is calculated by using a linear relationship between the stress σ and the strain δ (indentation) and strain rate $d\delta/dt$. Similarly to the approach used by Garcia *et al.*[45] to deduce a viscous force by combining Hertz and Voigt models, then

$$\sigma = E\delta + \eta\frac{d\delta}{dt} \quad (11)$$

an expression for the viscous force can be obtained by combining Tatara and Voigt models is given by

$$F_v \approx 0.35\eta\sqrt{R_{\text{eff}}\delta}\frac{d\delta}{dt} \quad (12)$$

where η is the viscosity coefficient. We considered two different cases characterized, respectively, by $\eta = 0$ and 100 Pa·s. Thus elastic and moderate viscoelastic materials are considered.

In the model, we have also introduced the forces given by the Derjaguin−Landau−Verwey−Overbeek (DVLO) model.[38] Although many molecular resolution experiments are usually performed in a high-ionic concentration buffer where DVLO forces are greatly screened,[47] the use of rather small amplitudes of 2 nm or less makes the Debye length (~0.5 nm) comparable to the oscillation amplitude. The DLVO forces are calculated by[43]

$$F_{\text{DLVO}} = \frac{4\pi R}{\varepsilon\varepsilon_0}\sigma_t\sigma_s\lambda_D\exp(-d/\lambda_D) - \frac{HR}{6d^2} \quad (13)$$

where σ_t, σ_s, ε, ε_0, λ_D, and H are, respectively, the surface charge density of the tip, the surface charge density of the sample, relative dielectric constant of the medium, dielectric constant of the vacuum, Debye length, and Hamaker constant. The simulations have been performed with $\sigma_t = 0.032$ C m^{-2} (ref 47), $\sigma_s = 0.05$ C m^{-2} (ref 47), $\varepsilon = 79$, $\varepsilon_0 = 8.85 \times 10^{-12}$ C^2 N^{-1} m^{-2}, $\lambda_D = 0.48$ nm, and $H = 0.5 \times 10^{-20}$ J.

Conflict of Interest: The authors declare no competing financial interest.

Acknowledgment. We thank the motivating discussions with Simon Scheuring. We thank the financial support from the Ministerio de Economía y Competitividad (Consolider Force-For-Future, CSD2010-00024, MAT2009-08650) and the EU project FP7-NMP-2011-280772 `Implantable Organic Nano-Electronics' (I-ONE) and the Cost Action TD1002.

REFERENCES AND NOTES

1. Gan, Y. Atomic and Subnanometer Resolution in Ambient Conditions by Atomic Force Microscopy. *Surf. Sci. Rep.* **2009**, *64*, 99–121.
2. Uchihashi, T.; Lino, R.; Ando, T.; Noji, H. High-Speed Atomic Force Microscopy Reveals Rotary Catalysis of Rotorless F(1)-ATPase. *Science* **2011**, *333*, 755–758.
3. Garcia, R.; Magerle, R.; Perez, R. Nanoscale Compositional Mapping with Gentle Forces. *Nat. Mater.* **2007**, *6*, 405–411.
4. Yamada, H.; Kobayashi, K.; Fukuma, T.; Hirata, Y.; Kajita, T.; Matsushige, K. Molecular Resolution Imaging of Protein Molecules in Liquid Using Frequency Modulation Atomic Force Microscopy. *Appl. Phys. Lett.* **2008**, *2*, 095007.
5. Higgings, M. J.; Sader, J. E.; Jarvis, S. P. Frequency Modulation Atomic Force Microscopy Reveals Individual Intermediates with Each Unfolded I27 Titin Domain. *Biophys. J.* **2006**, *90*, 640–647.
6. Voitchovsky, K.; Kuna, J. J.; Contera, S. A.; Tosatti, E.; Stellacci, F. Direct Mapping of the Solid−Liquid Adhesion with Subnanometer Resolution. *Nat. Nanotechnol.* **2010**, *5*, 401–405.
7. Dong, M.; Husale, S.; Sahin, O. Determination of Protein Structural Flexibility by Microsecond Force Spectroscopy. *Nat. Nanotechnol.* **2009**, *4*, 514–517.
8. Raman, A.; Trigueros, S.; Cartagena, A.; Stevenson, A. P. Z.; Susilo, M.; Nauman, E.; Contera, S. A. Mapping Nanomechanical Properties of Live Cells Using Multiharmonic Atomic Force Microscopy. *Nat. Nanotechnol.* **2011**, *6*, 809–814.
9. Xu, X.; Melcher, J.; Basak, S.; Reinferberger, R.; Raman, A. Compositional Contrast of Biological Materials in Liquid Using the Momentary Excitation of Higher Eigenmodes in Dynamic Atomic Force Microscopy. *Phys. Rev. Lett.* **2009**, *102*, 060801.
10. Ando, T.; Uchihashi, T.; Fukuma, T. High-Speed Atomic Force Microscopy for Nano-Visualization of Dynamic Biomolecular Processes. *Prog. Surf. Sci.* **2008**, *83*, 337–437.
11. Martinez-Martin, D.; Herruzo, E. T.; Dietz, C.; Gomez-Herrero, J.; Garcia, R. Noninvasive Protein Structural Flexibility Mapping by Bimodal Dynamic Force Microscopy. *Phys. Rev. Lett.* **2011**, *106*, 198101.
12. Rico, F.; Su, C.; Scheuring, S. Mechanical Mapping of Single Membrane Proteins at Submolecular Resolution. *Nano Lett.* **2011**, *11*, 3983–3986.
13. Mullin, N.; Hobbs, J. K. Direct Imaging of Polyethylene Films at Single-Chain Resolution with Torsional Tapping Atomic Force Microscopy. *Phys. Rev. Lett.* **2011**, *107*, 197801.
14. Han, W.; Lindsay, S. M.; Jing, T. A Magnetically Driven Oscillating Probe Microscope for Operation in Liquids. *Appl. Phys. Lett.* **1996**, *69*, 4111.
15. Revenko, I.; Proksch, R. Magnetic and Acoustic Tapping Mode Microscopy of Liquid Phase Phospholipids Bilayers and DNA Molecules. *J. Appl. Phys.* **2000**, *87*, 526–528.
16. Herruzo, E. T.; Garcia, R. Frequency Response of an Atomic Force Microscope in Liquids and Air: Magnetic *versus* Acoustic Excitation. *Appl. Phys. Lett.* **2007**, *91*, 143113.
17. Sekiguchi, H.; Okajima, T.; Arakawa, H.; Maeda, S.; Takashima, A.; Ikai, A. Frequency Shift Feedback Imaging in Liquid for Biological Molecules. *Appl. Surf. Sci.* **2003**, *210*, 61–67.
18. Hoogenboom, B. W.; Hug, H. J.; Pellmont, Y.; Martin, S.; Frederix, P. L. T. M.; Fotiadis, D.; Engel, A. Quantitative

Dynamic-Mode Scanning Force Microscopy in Liquid. *Appl. Phys. Lett.* **2006**, *88*, 193109.
19. Martinez, J.; Yuzvinsky, T. D.; Fennimore, A. M.; Zettl, A.; Garcia, R.; Bustamante, C. Length Control and Sharpening of Atomic Force Microscope Carbon Nanotube Tips Assisted by an Electron Beam. *Nanotechnology* **2005**, *16*, 2493.
20. Santos, S.; Guang, L.; Souier, T.; Gadelrab, K.; Chiesa, M.; Thomson, N. H. A Method to Provide Rapid *In Situ* Determination of Tip Radius in Dynamic Atomic Force Microscopy. *Rev. Sci. Instrum.* **2012**, *83*, 043707.
21. Santos, S.; Barcons, V.; Verdaguer, A.; Font, J.; Thomson, N. H.; Chiesa, M. How Localized Are Energy Dissipation Processes in Nanoscale Interactions?. *Nanotechnology* **2011**, *22*, 345401.
22. Garcia, R.; Herruzo, E. T. The Emergence of Multifrequency Force Microscopy. *Nat. Nanotechnol.* **2012**, *7*, 217–226.
23. San Paulo, A.; Garcia, R. High-Resolution Imaging of Antibodies by Tapping-Mode Atomic Force Microscopy: Attractive and Repulsive Tip−Sample Interaction Regimes. *Biophys. J.* **2000**, *78*, 1599–1605.
24. Muller, D. J.; Fotiadis, D.; Engel, A. Mapping Flexible Protein Domains at Subnanometer Resolution with the AFM. *FEBS Lett.* **1998**, *430*, 105–111.
25. Casuso, I.; Khao, J.; Chami, M.; Paul-Gilloteaux, P.; Husain, M.; Duneau, J. P.; Stahlberg, H.; Sturgis, J. N.; Scheuring, S. Characterization of the Motion of Membrane Proteins Using High Speed Atomic Force Microscopy. *Nat. Nanotechnol.* **2012**, *7*, 525–529.
26. Hölscher, H. Quantitative Measurement of Tip−Sample Interactions in Amplitude Modulation AFM. *Appl. Phys. Lett.* **2006**, *89*, 123109.
27. Lee, M. H.; Jhe, W. H. General Theory of Amplitude Modulation AFM. *Phys. Rev. Lett.* **2006**, *97*, 036104.
28. Hu, S.; Raman, A. Inverting Amplitude and Phase To Reconstruct Tip−Sample Interaction Forces in Tapping Mode AFM. *Nanotechnology* **2008**, *19*, 375704.
29. Katan, A. J.; van Es, M.; Oosterkamp, T. H. Quantitative Force *versus* Distance Measurements in Amplitude Modulation AFM: A Novel Force Inversion Technique. *Nanotechnology* **2009**, *20*, 165703.
30. Sader, J. E.; Uchihashi, T.; Higgins, M. J.; Farrell, A.; Nakayama, Y.; Jarvis, S. P. Quantitative Measurement of Salvation Shells Using Frequency Modulated Atomic Force Microscopy. *Nanotechnology* **2005**, *16*, S49–S53.
31. San Paulo, A.; Garcia, R. Tip-Surface Forces, Amplitude and Energy Dissipation in Amplitude Modulation (Tapping-Mode) Force Microscopy. *Phys. Rev. B* **2001**, *64*, 193411.
32. Legleiter, J.; Park, M.; Cusick, B.; Kowalewski, T. Scanning Probe Acceleration Microscopy (SPAM) in Fluids: Mapping Mechanical Properties of Surfaces at the Nanoscale. *Proc. Natl. Acad. Sci. U.S.A.* **2006**, *103*, 4813–4818.
33. Hu, S.; Raman, A. Analytical Formulas and Scaling Laws for Peak Interaction Forces in Dynamic Atomic Force Microscopy. *Appl. Phys. Lett.* **2007**, *91*, 123106.
34. Xu, X.; Carrasco, C.; de Pablo, P. J.; Gomez-Herrero, J.; Raman, A. Unmasking Imaging Forces on Soft Biological Samples in Liquids: Case Study on Viral Capsids. *Biophys. J.* **2008**, *95*, 9520.
35. Xu, X.; Melcher, J.; Raman, A. Accurate Force Spectroscopy in Tapping Mode Atomic Force Microscopy in Liquids. *Phys. Rev. B* **2010**, *81*, 035407.
36. Kumar, B.; Pifer, P. M.; Giovengo, A.; Legleiter, J. The Effect of the Set Point Ratio and Surface Young's Modulus on Maximum Tapping Forces in Fluid Tapping Mode Force Microscopy. *J. Appl. Phys.* **2010**, *107*, 044508.
37. Solares, S. D.; Chang, J.; Seong, J.; Kareem, A. U. Utilization of Simple Scaling Laws for Modulating Tip−Sample Peak Forces in Atomic Force Microscopy Characterization in Liquid Environments. *J. Appl. Phys.* **2011**, *110*, 094904.
38. Butt, H. J.; Kappl, M. Surface and Interfacial Forces; Wiley-VCH Verlag GmbH & Co. KGaA: Weinheim, Germany, 2010; pp 117−119.
39. Tatara, Y. Extensive Theory of Force-Approach Relations of Elastic Spheres in Compression and in Impact. *J. Eng. Mater. Technol.* **1989**, *111*, 163–168.
40. Tatara, Y. Large Deformations of a Rubber Sphere under Diametral Compression. *JSME Int. J.* **1993**, *36*, 190–196.
41. Ikai, A. The World of Nano-Biomechanics; Elsevier B.V.: Amsterdam, The Netherlands, 2008; pp 148−154.
42. Kodera, N.; Yamamoto, D.; Ishikawa, R.; Ando, T. Video Imaging of Walking Myosin V by High-Speed Atomic Force Mciroscopy. *Nature* **2010**, *468*, 72–76.
43. Garcia, R. Amplitude Modulation Atomic Force Microscopy; Wiley-VCH Verlag GmbH & Co. KGaA: Weinheim, Germany, 2010; pp 56−57.
44. San Paulo, A.; Garcia, R. Unifying Theory of Tapping-Mode Atomic Force Microscopy. *Phys. Rev. B* **2002**, *66*, 041406(R).
45. Garcia, R.; Gomez, C. J.; Martinez, N. F.; Patil, S.; Dietz, C.; Magerle, R. Identification of Nanoscale Processes by Dinamic Atomic Force Microscopy. *Phys. Rev. Lett.* **2006**, *97*, 16103.
46. Payam, A. F.; Ramos, J. R.; Garcia, R. Molecular and Nanoscale Compositional Contrast of Soft Matter in Liquid: Interplay between Elastic and Dissipative Interactions. *ACS Nano* **2012**, *6*, 4663–4670.
47. Muller, D. J.; Fotiadis, D.; Scheuring, S.; Muller, S. A.; Engel, A. Electrostatically Balanced Subnanometer Imaging of Biological Specimens by Atomic Force Microscope. *Biophys. J.* **1999**, *76*, 1101–1111.